Combining Bottom-Up Self-Assembly with Top-Down Microfabrication to Create Hierarchical Inverse Opals with High Structural Order

*Manuel Schaffner, Grant England, Mathias Kolle, Joanna Aizenberg, and Nicolas Vogel**

Colloidal particles can assemble into ordered crystals, creating periodically structured materials at the nanoscale without relying on expensive equipment. The combination of small size and high order leads to strong interaction with visible light, which induces macroscopic, iridescent structural coloration. To increase the complexity and functionality, it is important to control the organization of such materials in hierarchical structures with high degrees of order spanning multiple length scales. Here, a bottom-up assembly of polystyrene particles in the presence of a silica sol–gel precursor material (tetraethylorthosilicate, TEOS), which creates crack-free inverse opal films with high positional order and uniform crystal alignment along the (110) crystal plane, is combined with top-down microfabrication techniques. Micrometer scale hierarchical superstructures having a highly regular internal nanostructure with precisely controlled crystal orientation and wall profiles are produced. The ability to combine structural order at the nano- and microscale enables the fabrication of materials with complex optical properties resulting from light–matter interactions at different length scales. As an example, a hierarchical diffraction grating, which combines Bragg reflection arising from the nanoscale periodicity of the inverse opal crystal with grating diffraction resulting from a micrometer scale periodicity, is demonstrated.

M. Schaffner, G. England, Prof. J. Aizenberg
School of Engineering and Applied Sciences
Harvard University
9 Oxford Street, Cambridge, MA 02139, USA
Prof. M. Kolle
Department of Mechanical Engineering
Massachusetts Institute of Technology
77 Massachusetts Avenue, Cambridge, MA 02139, USA
Prof. N. Vogel
Institute of Particle Technology
Friedrich-Alexander-University Erlangen-Nürnberg
Haberstr. 9a, 91058 Erlangen, Germany
E-mail: nicolas-vogel@fau.de
Prof. N. Vogel
Cluster of Excellence Engineering of Advanced Materials
Friedrich-Alexander-University Erlangen-Nürnberg
Nägelsbacherstr. 49, 91054 Erlangen, Germany

DOI: 10.1002/smll.201500865

1. Introduction

Colloidal self-assembly is widely appreciated as an experimentally simple, low-tech process to create well-defined nanostructures.[1–3] Owing to their high order and periodicity at a length scale comparable to the wavelengths contained in the optical spectrum, colloidal crystals can interact strongly with visible light. The periodic modulation of the refractive index in opaline materials gives rise to a photonic bandgap, which results in high intensities of reflected light in the wavelength range corresponding to the range of frequencies within the bandgap. The position of the bandgap can be varied, for example, by changing the size of the colloidal particles used in the crystal's creation or by altering composition or shape.[4–6] Moreover, colloidal crystals can be used as sacrificial templates to fabricate inverse opals. Like their direct opal analogues, inverse opals possess interesting optical

properties and have been extensively used in photonic applications.[4–8] The well-defined, interconnected porosity at the nanoscale further allows for applications in various fields, including wetting,[9–12] (photo)catalysis,[13,14] cell culturing,[15] photovoltaics,[16,17] energy storage,[18–20] and sensing.[5,9,21,22] Most of these applications simplistically utilize inverse opals as thin films.

Precise spatial control of colloidal assemblies in hierarchical structures spanning multiple length scales can enable more advanced applications, for example, multiplexed and miniaturized sensing devices,[23] pixelated arrays of structural color units,[24–26] miniaturized photonic elements,[27] or microstructured electrodes with high surface area.[19] Furthermore, a hierarchical design may enable us to alter or to enhance the optical properties of such self-assembled structures by combination of the photonic bandgap properties with reflective, scattering or dispersive elements, with a potential to mimic complex structural colors found in nature.[28,29]

The assembly of hierarchical colloidal crystal structures can be controlled from the bottom up by prepatterning the substrate with a desired topography.[30–36] If the topography is chosen to match the symmetry of the colloidal crystal, highly ordered, hierarchical structures result.[33,36,37] If the imposed topography interferes with the overall lattice orientation, the crystal growth is frustrated, leading to disorder and cracks.[36] As a consequence, the quality of the crystal is significantly reduced.

If the order in the colloidal assembly is to be maintained for any desired structural feature, the assembly process must be separated from the patterning. This can be achieved by using top-down, microfabrication techniques such as photolithography,[25,38–40] microcontact printing, imprinting and stamping,[26,41,42] or inkjet printing.[43] In these approaches, defects in the crystal structures can be created by curvature or patterning protocols, be inherited from the assembly process or mechanical treatment and include polycrystallinity arising from different nucleation sites, cracks and over- or underfilled pores when replicated into inverse structures.

Here, we use a coassembly method to crystallize polymer colloids in the presence of tetraethylorthosilicate (TEOS), which has been shown to result in well ordered inverse opal thin films with open and interconnected pores and low density of cracks at square centimeter dimensions and beyond.[44] Most remarkably, the assembled structures show single crystal orientation throughout the substrate arising from a preferred growth along the (110) crystal plane.[36,44] To preserve the order, we apply photolithography and reactive ion beam etching in a post-assembly step to fabricate arbitrarily shaped hierarchical superstructures and patterns that possess an equally high degree of order and crystal orientation.

2. Results and Discussion

Figure 1A schematically shows the fabrication of the hierarchical inverse opal superstructure. We crystallize polystyrene colloidal particles by evaporative assembly in the presence of a silica sol–gel precursor (TEOS). After calcination at

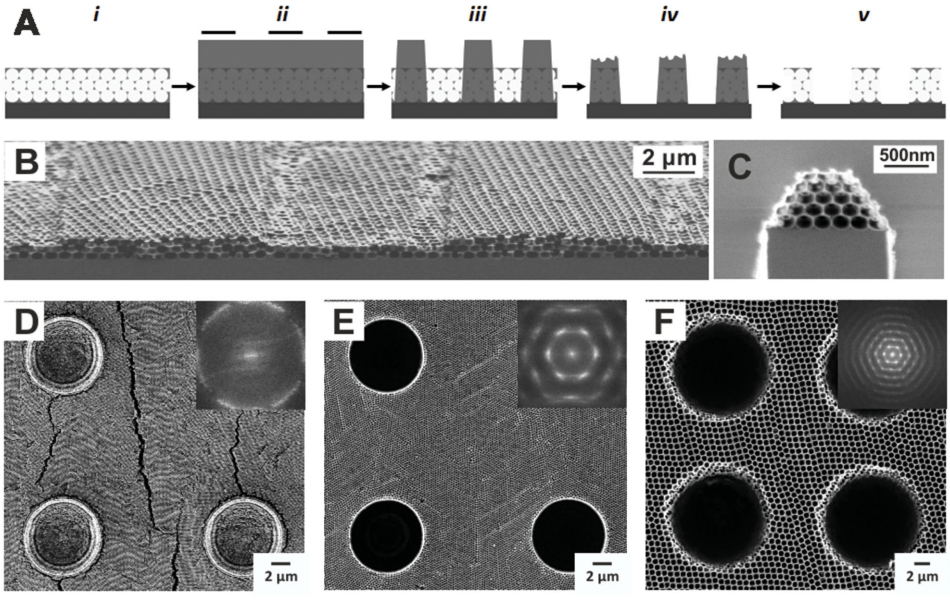

Figure 1. Decoupling the crystal formation from patterning creates hierarchical structures with uncompromised order. A) Schematic illustration of superstructure fabrication. A highly ordered inverse opal (i) is infiltrated with photoresist and exposed to UV light to create a pattern (ii). The inverse opal/photoresist hybrid structure is developed, removing the photoresist from the porous structure at the exposed substrate areas (iii). Anisotropic reactive ion beam etching is used to remove all unprotected parts of the opal (iv). After calcination to remove photoresist, the inverse opal superstructure is formed (v). B) Patterned inverse opal with a step size of one colloidal layer, demonstrating high vertical resolution. C) Side-view image of an inverse opal line pattern, showing vertical etching along the (111) plane of the crystal. D–F) Comparison of the order in hierarchical structures obtained by assembling a direct opal on a lithographically patterned substrate with topography (D), co-assembling colloids in the presence of TEOS on a similarly patterned substrate to create a hierarchical inverse opal (E), and by decoupling the crystal formation from the lithographic patterning step, following the procedures described in the current paper (F). The crystal order is completely preserved if the patterning step is applied after crystal formation.

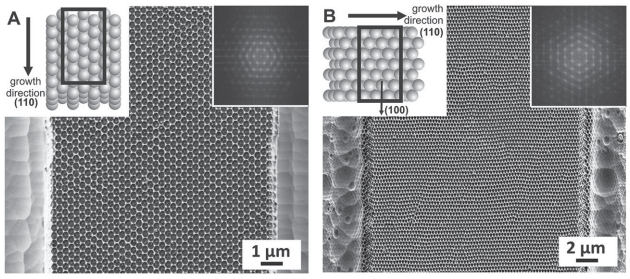

Figure 2. Control of crystal orientation within the superstructure. The inverse opal thin films preferentially grow along the (110) direction (see insets). Any arbitrary orientation of the constituent photonic crystal within the final hierarchical pattern can be achieved by simple rotation of the mask relative to the orientation of the substrate. A) When a pattern (black box) is aligned along the growth direction, hierarchical structures with a (110) orientation of the inverse opal crystal within the superstructure form; B) Aligning the pattern perpendicular to the growth direction yields hierarchical structures with a (100) orientation. High order and uniform orientation are evident from the FFT images shown as insets.

500 °C, we obtain a highly ordered, iridescent inverse opal thin film with oriented crystallinity throughout the substrate.[36,44] We then infuse the porous matrix with a photoresist that has a refractive index closely matching that of the surrounding silica. The resulting infiltration of the pores by the resist is indicated by the disappearance of the iridescence.[9,45] The resist-filled inverse opal is UV-exposed through a mask with the desired structural pattern. Since the pores are all filled with the index-matched photoresist, scattering of UV-light is prevented, leading to high quality photolithographic patterns without blurring of features. We thus create a protective photoresist layer covering selected parts of the substrate. Anisotropic reactive ion beam etching is then used to mill into the substrate, removing the inverse opal structures at all unprotected areas. In a final calcination step, photoresist residues are removed, yielding a pattern of highly ordered, inverse opal superstructures.

The etching depth can be precisely controlled via the etching time, allowing us to remove individual layers of the inverse opal (Figure 1B). The minimum obtainable feature sizes are defined by the resolution of photolithography and the reactive ion beam etching step: for straight line patterns, we find a selective vertical etching along the (111) cleavage plane of the substrate to produce a characteristic trapezoidal wall profile (Figure 1C), which we attribute to the minimal amount of mass that needs to be removed along that plane. This etching characteristic leads to 60° vertical incline at the edges, giving us a reproducible three-dimensional morphology of the patterned inverse opal. Simple geometric considerations (Supporting Information) allow us to determine the lateral resolution of the hierarchical inverse opal feature x as a function of the inverse opal layer thickness h and the lateral size of the photoresist pattern used as a mask x(lithography):

$$x(h) = x(\text{lithography}) + \left(2/\sqrt{3}\right)h$$

Figure 1D–F compares the degree of order in hierarchical colloidal assemblies prepared by self-assembling direct (Figure 1D) and inverse opals (Figure 1E) on substrates with a topography, and by top-down patterning of prefabricated inverse opals (Figure 1F). As we have observed previously, the co-assembly of colloids with TEOS increases long-range order and eliminates crack formation (Figure 1E) as compared to a direct assembly of colloids (Figure 1D).[36] However, since the geometry of the topography does not match the crystal structure, the co-assembled crystal shown in Figure 1E shows frustrated crystallization, creating disorder around the obstacle. In contrast, the high order and orientation of the crystal is completely retained when assembly and patterning are separated (Figure 1F).

The preferential growth of the co-assembled colloidal crystal film along the (110) plane generates inverse opal films with high crystal alignment,[36,44] which can be transferred into the hierarchical pattern by aligning the photolithography mask at a controlled angle (e.g. parallel or perpendicular to the growth direction of the inverse opal crystal) to create identical macroscopic patterns with various crystallographic orientations of the constituent self-assembled photonic crystal. **Figure 2** shows slabs of inverse opals with crystal orientations along the (110) plane and (100) plane, respectively. The insets show the orientation of the inverse opal film as grown on the substrate and the resulting orientation of the crystal within the pattern. The Fourier transformations, showing undisturbed hexagonal patterns, indicate high order and crystal alignments.

The process allows the creation of complex, arbitrarily shaped hierarchical structures with high accuracy and resolution while maintaining order and orientation of the inverse opal crystal, which we demonstrate by a micrometer scale reproduction of a world map (**Figure 3**A). The map, with its

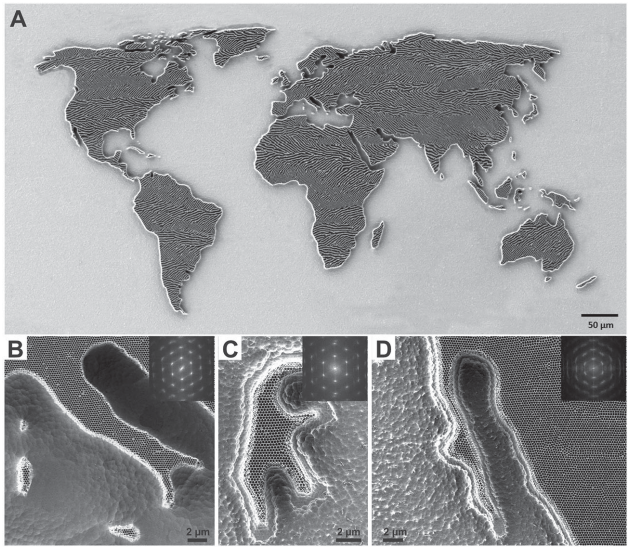

Figure 3. Fabrication of single crystalline, complex patterns with hierarchical features spanning multiple length scales. A) SEM image of a micrometer scale inverse opal pattern in the shape of the world map. The Moiré patterns visible throughout the image indicate high order. B–E) Close-up SEM images and Fourier transformation analyses (insets) of different parts of the world map. The images show (B) Italy, (C) Sulawesi, and (D) the Baja California peninsula. Order and uniform crystal orientation in images are evident from Fourier transformation (insets).

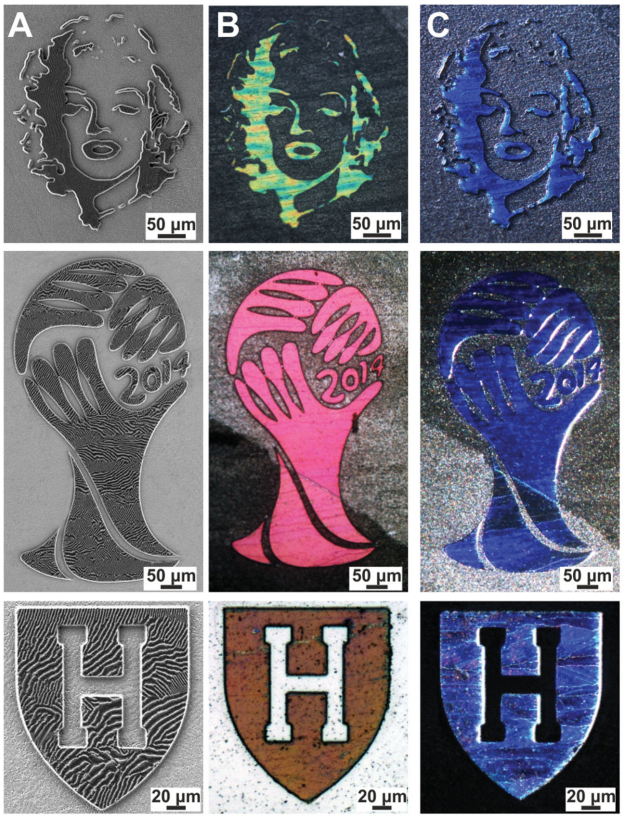

Figure 4. Structural color imaging at micrometer scale. A) SEM images of hierarchical inverse opal structures; microscopy images taken (B) with illumination normal and (C) off-normal to the surface. The images show real, dynamic structural color that blue-shifts with increasing illumination angle.

complex shape, demonstrates our ability to pattern arbitrary features with multiple length scales—including adjacent concave and convex features. Moiré patterns, indicative of high crystal order,[46] are visible throughout the image. Order and crystal alignment throughout the complete structure is further highlighted in high magnification images of selected regions (Figure 3B–D), which all show uniform crystal alignment resulting from the single crystal orientation of the underlying coassembled inverse opal. This uniform alignment of the crystal is evidenced by Fourier transform analyses shown as insets. The specific crystallographic orientation of the inverse opal single crystal in the pattern can be altered by rotation of the imposed photolithographic mask with respect to the substrate (compare, for example, two perpendicular orientations of the line pattern in the [110] and [100] directions in Figure 2). The lateral resolution achieved in some parts of the map is below 1 μm—only a few colloidal particles in width.

Since the order of the colloidal assembly is retained in the generated hierarchical structures, they also maintain their distinctive structural coloration. The wavelength of constructive interference changes with the incident angle, giving the inverse opals their vivid iridescence. This color shift allows us to create complex, micrometer scale structures with dynamic coloration (**Figure 4**). We design arbitrary, micrometer scale "artworks" and illuminate the structure under a microscope. With an illumination normal to the surface, the structures show green (top, 250 nm colloids used as template) and red colors (middle, bottom, 320 nm colloids) depending on the size of the colloids (Figure 4B). The variation of color in the top image of Figure 4B arises from changes in crystal thickness.[9] As expected, the observed color shifts into the blue part of the spectrum with increasing light incidence angles (Figure 4C). Additional levels of complexity may be introduced to the system by tailoring liquid infiltration by means locally changing the surface chemistry[45] or locally modifying the color by changing the pore sizes, for example using atomic layer deposition.

The hierarchical microfabrication allows the combination of photonic effects occurring on disparate length scales. For example, we can create a hierarchical diffraction grating by patterning inverse opals into periodic stripes (**Figure 5**A,B). A diffraction grating creates an angular dispersion of light

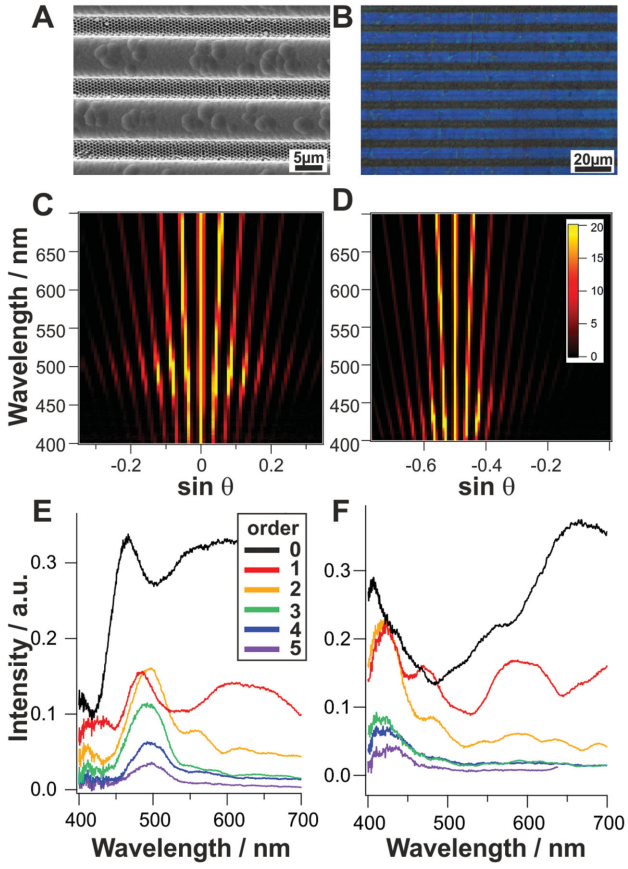

Figure 5. Multiple optical properties arise from periodicities at different length scales in hierarchical inverse opal structures. A) SEM and B) optical microscope image of periodically spaced inverse opal slabs serving as a hierarchical diffraction gratings. C,D) Optical properties of the inverse opal diffraction grating represented in two dimensions by plotting the sine of the reflected light versus the wavelength. Each vertical line represents an individual spectrum. The spectra were taken for (C) incident light normal to the surface and (D) at an angle of 30° relative to the surface normal. The hierarchical structure shows multiple diffraction orders, visible as straight lines in the figure. E,F) Wavelength-dependent intensity, taken along the first five diffraction orders. As a result of the inverse opal structure, the light intensity in these individual orders is modulated and shows enhanced intensity at the Bragg diffraction peak, which shifts with increasing incident light angle.

(with a wavelength λ) dependent on the illumination conditions (angle of incident light θ_i and diffracted light θ_d) and the periodicity d of the grating as described by the grating equation:[47]

$$m\lambda = d(\sin\theta_i + \sin\theta_d)$$

We investigate the optical properties of our hierarchical diffraction grating by variable angle spectroscopy, measuring reflection spectra as a function of observation angle over a wide range of angles. Figure 5C,D shows the reflected light intensity for all measured wavelengths and diffraction angles (plotted as $\sin(\theta)$ for better comparison with the grating equation). The data are plotted as an image with vertical columns corresponding to spectra measured at each detection angle and rows corresponding to the wavelengths detected by the spectrometer. Intensity of the reflected light is color-coded with black signifying low and yellow high intensities. The incidence angles shown are 0° and 30° for Figure 5C,D. Multiple diffraction orders, arising from the *microscale* periodicity of the superstructure are visible as straight lines in the plots.

The distribution of light intensity in the individual diffraction orders shows the fingerprint of the second optical element present in the hierarchical material—the inverse opal. The photonic bandgap, arising from the *nanoscale* periodicity of the colloidal crystal, is encoded in all individual diffraction orders and, as expected, blue-shifts with increasing angle of incident light. In Figure 5C, enhanced reflected intensity is detected around 500 nm for all diffraction orders. This signature of the Bragg diffraction peak shifts toward 420 nm when the angle of incident light is changed (Figure 5D). Figure 5E,F presents the wavelength-dependent intensity, extracted along the first five positive diffraction orders for both incident angles. Again, the incident angle-sensitive signature of the Bragg diffraction peak is clearly visible at 500 nm (0° incident light, Figure 5E) and 420 nm (30° incident light, Figure 5F) in all diffraction orders.

3. Conclusions

In conclusion, we have exploited the high order and single crystal orientation found in inverse opals assembled from polymeric colloids in the presence of TEOS to create superstructures by a combination of photolithography and reactive ion beam etching of the pre-assembled, crystallographically oriented inverse opal films. The uniform crystal orientation across the entire patterned area remains unaltered in the produced, highly ordered hierarchical structures and can be controlled by orienting the lithographic pattern at an arbitrary angle relative to the underlying single crystal. This enables us to align different crystal planes within the individual hierarchical elements. In addition to the resolution of the lithographic procedure, the minimal structural feature width (coupled with the feature height) is limited by the anisotropic trapezoidal etch mechanism that follows (111) cleavage planes of the crystal. These hierarchical patterns show angular-dependent structural coloration which we exploit to create iridescent real color images at a micrometer scale. Furthermore, the control of order and periodicity at multiple length scales allows creating materials that combine multiple optical properties. We demonstrate such complex optical materials by encoding the photonic bandgap properties within the individual diffraction orders of a diffraction grating. We believe that the controlled fabrication of high-quality inverse opal superstructures with full control of feature sizes, controlled crystal orientation, and minimum defect density will open pathways to harvest the intriguing properties of inverse opals in advanced applications and devices—from miniaturized sensing architectures to a sophisticated tailoring of light-matter interactions in photonics or phononics. Especially, we anticipate the technology to serve as an experimentally simple platform to create multi-scale optical materials to help understand and mimic the vivid coloration of hierarchical structures occurring in nature.

4. Experimental Section

Preparation of Inverse Opals: Polystyrene (PS) colloids were synthesized using a surfactant-free emulsion polymerization following a protocol from literature.[48] Inverse opals were synthesized by a coassembly process with TEOS.[44] PS colloids were added to 20 mL of water and adjusted to 0.1% solid content. 150 µL of prehydrolyzed TEOS solution (1:1:1.5 by volume of TEOS:0.1 M HCl:ethanol, stirred for 1 h at room temperature) was added and the mixture was sonicated for 5 min. A cleaned silicon wafer (exposed to acid piranha for 45 min and extensively rinsed with water) was vertically suspended in the vial and placed inside the oven for several days for the solvent to evaporate completely. A vibration-free oven set to 65 °C was used for the coassembly process. After complete solvent evaporation, a single-domain opal film with silicon dioxide filling the interstitials was left on the wafer substrate. Calcination for 5 h at 500 °C with a defined heating ramp of 2 °C min^{-1} and a cooling time to room temperature in 3 h resulted in high quality inverse opal film. Deionized water was used from a Milli-Q system, ethanol was purchased from Koptec, and all other chemicals were purchased from Sigma-Aldrich.

Photolithography on Inverse Opal Film: Photolithography was performed in an ISO class 5 clean room at CNS, Harvard. Inverse opal films were cleaned with acetone and isopropyl alcohol (IPA) on a Headway Research spin coater at 3000 rpm for 10 s each. Complete solvent evaporation was performed on a Torrey Pines hot plate at 180 °C for 5 min. Samples were then pre-coated with hexamethyl disilazane (HMDS) at 3000 rpm for 60 s and soft baked at 110 °C for 60 s. Thereafter, Shipley S1818 positive photoresist was spin coated on the sample at 2000 rpm for 45 s and hard baked at 110 °C for 60 s, giving a protective layer thickness of 2 µm. Chrome masks were designed with AutoCAD 2014 and printed using a Heidelberg DWL 66 mask writer. Using a Suss MJB4 mask aligner, soft-contact (1.3 bar) was established between the chrome mask and the coated sample. Exposure time was calculated by dividing the exposure dose E_0 (180 mJ cm^{-2} for S1818) by the h-line intensity (405 nm) of the MJB4 mask aligner. Standard exposure time was 4.5 s. For feature sizes smaller than 6 µm, additional 0.1 s were added to the calculated exposure time for every 1 µm decrease

in size. After exposure, samples were hard baked at 110 °C for 60 s and developed with Microposit MF CD-26 developer. Developing steps were first 50 s in CD-26, followed by 10 s in fresh CD-26 and 15 s in DI water. Samples were blow dried with nitrogen.

Reactive Ion Etching: Anisotropic reactive ion etching was performed on a STS induced coupled plasma reactor (STS ICP RIE) with a standard recipe for silicon dioxides etch. The plasma reactor was first cleaned with oxygen plasma for 20 min, followed by a 10 min stabilization cycle of the etch program. 10 sccm C_4F_8, 10 sccm SF_6 and 3 sccm H_2 were used with 900 W coil power, 100 W platen power at 7 mTorr and 38 °C. Etch rates were determined by a Veeco Dektak profilometer. We found etch rates of 0.43 μm min^{-1} for inverse opal and 0.35 μm min^{-1} for photoresist, giving an etching ratio of 1:1.23 resist to inverse opal. Samples were rinsed with ethanol and IPA. To remove the protective photoresist layer, the samples were calcined for 5 h at 500 °C with a defined heating ramp of 2 °C min^{-1} and a 3 h cooling time back to room temperature.

Imaging and Characterization: Scanning electron microscopy (SEM) was performed on a Zeiss Ultra Plus field emission microscope. ImageJ was used for subsequent image analysis. An Ocean Optics DH-2000 UV–vis–NIR light source was used for the variable angle spectrometry measurements to illuminate a small spot (<1 mm) on the sample at a given incidence angle. Individual spectra were collected at half degree increments for −75° to +75° relative to the sample normal for each angle of illumination and spectrally analyzed using an Ocean Optics Maya Pro 2000 spectrometer.

Supporting Information

Supporting Information is available from the Wiley Online Library or from the author.

Acknowledgements

This work was supported by the National Science Foundation (NSF) Materials Research Science and Engineering Centers (MRSEC) at Harvard University under Award No. DMR 14–20570. N.V. acknowledges funding from the Cluster of Excellence - Engineering of Advanced Materials.

[1] G. von Freymann, V. Kitaev, B. V. Lotsch, G. A. Ozin, *Chem. Soc. Rev.* **2013**, *42*, 2528.
[2] F. Li, D. P. Josephson, A. Stein, *Chem.-Int. Ed.* **2011**, *50*, 360.
[3] T. Kraus, D. Brodoceanu, N. Pazos-Perez, A. Fery, *Adv. Funct. Mater.* **2013**, *23*, 4529.
[4] C. I. Aguirre, E. Reguera, A. Stein, *Adv. Funct. Mater.* **2010**, *20*, 2565.
[5] A. C. Arsenault, T. J. Clark, G. Von Freymann, L. Cademartiri, R. Sapienza, J. Bertolotti, E. Vekris, S. Wong, V. Kitaev, I. Manners, R. Z. Wang, S. John, D. Wiersma, G. A. Ozin, *Nat. Mater.* **2006**, *5*, 179.
[6] K. R. Phillips, N. Vogel, Y. Hu, M. Kolle, C. C. Perry, J. Aizenberg, *Chem. Mater.* **2014**, *26*, 1622.
[7] A. C. Arsenault, D. P. Puzzo, I. Manners, G. A. Ozin, *Nat. Photonics* **2007**, *1*, 468.
[8] Y. Y. Diao, X. Y. Liu, *Adv. Funct. Mater.* **2012**, *22*, 1354.
[9] I. B. Burgess, N. Koay, K. P. Raymond, M. Kolle, M. Loncar, J. Aizenberg, *ACS Nano* **2012**, *6*, 1427.
[10] N. Vogel, R. A. Belisle, B. Hatton, T. S. Wong, J. Aizenberg, *Nat. Commun.* **2013**, *4*, 2167.
[11] K. R. Phillips, N. Vogel, I. B. Burgess, C. C. Perry, J. Aizenberg, *Langmuir* **2014**, *30*, 7615.
[12] J. X. Wang, Y. Z. Zhang, S. T. Wang, Y. L. Song, L. Jiang, *Acc. Chem. Res.* **2011**, *44*, 405.
[13] J. I. L. Chen, G. von Freymann, S. Y. Choi, V. Kitaev, G. A. Ozin, *Adv. Mater.* **2006**, *18*, 1915.
[14] J. Liu, G. Liu, M. Li, W. Shen, Z. Liu, J. Wang, J. Zhao, L. Jiang, Y. Song, *Energy Environ. Sci.* **2010**, *3*, 1503.
[15] S.-W. Choi, J. Xie, Y. Xia, *Adv. Mater.* **2009**, *21*, 2997.
[16] S. Guldin, S. Hüttner, M. Kolle, M. E. Welland, P. Müller-Buschbaum, R. H. Friend, U. Steiner, N. Tétreault, *Nano Lett.* **2010**, *10*, 2303.
[17] N. Tétreault, É. Arsenault, L.-P. Heiniger, N. Soheilnia, J. Brillet, T. Moehl, S. Zakeeruddin, G. A. Ozin, M. Grätzel, *Nano Lett.* **2011**, *11*, 4579.
[18] A. Esmanski, G. A. Ozin, *Adv. Funct. Mater.* **2009**, *19*, 1999.
[19] J. H. Pikul, H. Gang Zhang, J. Cho, P. V. Braun, W. P. King, *Nat. Commun.* **2013**, *4*, 1732.
[20] O.-H. Kim, Y.-H. Cho, S. H. Kang, H.-Y. Park, M. Kim, J. W. Lim, D. Y. Chung, M. J. Lee, H. Choe, Y.-E. Sung, *Nat. Commun.* **2013**, *4*, 2473.
[21] C. Fenzl, T. Hirsch, O. S. Wolfbeis, *Angew. Chem. Int. Ed.* **2014**, *53*, 3318.
[22] P. M. Tessier, O. D. Velev, A. T. Kalambur, J. F. Rabolt, A. M. Lenhoff, E. W. Kaler, *J. Am. Chem. Soc.* **2000**, *122*, 9554.
[23] Z. Xie, K. Cao, Y. Zhao, L. Bai, H. Gu, H. Xu, Z.-Z. Gu, *Adv. Mater.* **2013**, *26* , 2413.
[24] S. H. Kim, J. M. Lim, W. C. Jeong, D. G. Choi, S. M. Yang, *Adv. Mater.* **2008**, *20*, 3211.
[25] S. Y. Lee, S.-H. Kim, H. Hwang, J. Y. Sim, S.-M. Yang, *Adv. Mater.* **2014**, *26*, 2391.
[26] T. Ding, S. K. Smoukov, J. J. Baumberg, *Nanoscale* **2015**, *7*, 1857.
[27] S.-H. Kim, H. S. Park, J. H. Choi, J. W. Shim, S.-M. Yang, *Adv. Mater.* **2010**, *22*, 946.
[28] P. Vukusic, J. R. Sambles, *Nature* **2003**, *424*, 852.
[29] M. Kolle, U. Steiner, in *Encyclopedia of Nanotechnology* (Ed.: B. Bhushan), Springer, Netherlands **2012**.
[30] A. van Blaaderen, R. Ruel, P. Wiltzius, *Nature* **1997**, *385*, 321.
[31] J. Aizenberg, P. V. Braun, P. Wiltzius, *Phys. Rev. Lett.* **2000**, *84*, 2997.
[32] G. A. Ozin, S. M. Yang, *Adv. Funct. Mater.* **2001**, *11*, 95.
[33] S. M. Yang, H. Miguez, G. A. Ozin, *Adv. Funct. Mater.* **2002**, *12*, 425.
[34] C. A. Fustin, G. Glasser, H. W. Spiess, U. Jonas, *Langmuir* **2004**, *20*, 9114.
[35] T. Ding, L. Luo, H. Wang, L. Chen, K. Liang, K. Clays, K. Song, G. Q. Yang, C. H. Tung, *J. Mater. Chem.* **2011**, *21*, 11330.
[36] L. Mishchenko, B. Hatton, M. Kolle, J. Aizenberg, *Small* **2012**, *8*, 1904.
[37] E. Kumacheva, R. K. Golding, M. Allard, E. H. Sargent, *Adv. Mater.* **2002**, *14*, 221.
[38] P. Jiang, M. J. McFarland, *J. Am. Chem. Soc.* **2004**, *126*, 13778.
[39] S. K. Lee, G. R. Yi, J. H. Moon, S. M. Yang, D. J. Pine, *Adv. Mater.* **2006**, *18*, 2111.
[40] H. S. Lee, T. S. Shim, H. Hwang, S. M. Yang, S. H. Kim, *Chem. Mater.* **2013**, *25*, 2684.
[41] J. M. Yao, X. Yan, G. Lu, K. Zhang, X. Chen, L. Jiang, B. Yang, *Adv. Mater.* **2004**, *16*, 81.
[42] T. Ding, Q. B. Zhao, S. K. Smoukov, J. J. Baumberg, *Adv. Opt. Mater.* **2014**, *2*, 1098.

[43] J. X. Wang, L. B. Wang, Y. L. Song, L. Jiang, *J. Mater. Chem. C* **2013**, *1*, 6048.
[44] B. Hatton, L. Mishchenko, S. Davis, K. H. Sandhage, J. Aizenberg, *Proc. Natl. Acad. Sci. U. S. A.* **2010**, *107*, 10354.
[45] I. B. Burgess, L. Mishchenko, B. D. Hatton, M. Kolle, M. Lončar, J. Aizenberg, *J. Am. Chem. Soc.* **2011**, *133*, 12430.
[46] H. Hashimoto, R. Uyeda, *Acta Crystallog.* **1957**, *10*, 143.
[47] C. Palmer, *Diffraction Grating Handbook*, Newport Corporation, Rochester, New York **2005**.
[48] N. Vogel, L. de Viguerie, U. Jonas, C. Weiss, K. Landfester, *Adv. Funct. Mater.* **2011**, *21*, 3064.

Received: March 30, 2015
Revised: May 10, 2015
Published online: June 3, 2015